Effect of iron doping on structural, microstructural and gas sensing properties of nanocrystalline $ZnSnO_3$ thin films prepared by spray pyrolysis techniques

Idris G. Pathan [*], Dinesh N. Suryawanshi [1], Anil R. Bari[2], Lalchand A. Patil[3]

[*]Department of Physics, Arts, Commerce and Science College, Navapur, Maharashtra, India

[1]Department of Physics, Rani Laxmibai College, Parola, Maharashtra, India

[2]Department of Physics, Arts, Commerce and Science College, Bodwad, Maharashtra, India

[3]Nanomaterials Research Laboratory, Department of Physics, Pratap College, Amalner, Maharashtra, India

Abstract

This work presents the effect of iron doping on the structural, microstructural and electrical properties of zinc stannate ($ZnCl_4 \cdot 5H_2O$, 99.9% pure, Merck made, Germany) thin films, prepared by spray pyrolysis method. The thin films were prepared by doping ferric chloride ($FeCl_3 \cdot 4H_2O$, 99.9% pure, Merck made, Germany) having three different small volume ratios: 1 ml, 2.5 ml and 5 ml, in order to study the iron doping dependence of the structural and microstructural properties of thin films. These properties were characterized with X-ray diffraction (XRD) and Transmission Electron Microscope (TEM). In our study, XRD pattern indicates that $ZnSnO_3$ has a perovskite phase with face exposed hexahedron structure. The 2.5 vol % iron doped $ZnSnO_3$ thin films exhibited better gas response and rapid response–recovery characteristics to hydrogen. Further, it has been shown the gas sensitivity of the iron doped $ZnSnO_3$ gas sensor depends upon its grain size.

Keywords: pervoskite oxide, effect of iron doping, electrical properties, spray pyrolysis process.

1. Introduction

Recently, some composite oxides such as spinel AB_2O_4 and perovskite ABO_3 were found to be more attractive than single-metal oxides for their better selectivity and/or sensitivity to certain gases. Zinc stannate or zinc tin oxide (ZTO) is a class of ternary oxides that are known for their stable properties under extreme conditions and are useful for electrical as well as optical properties [1-6]. Zinc oxide (ZnO) has attracted attention because of the wide range of applications [7-10]. ZnO has been extensively investigated as a gas sensing material for practical applications. Generally, ZnO sensors provide a wide variety of advantages, such as low cost, short response time, easy manufacturing, and small in size, compared with the traditional analytical instruments. However, the traditional ZnO gas sensors suffer from several problems such as high operating temperature, poor selectivity, and relatively low response, which limit their applications

in real-time gas sensing. Doping is an important and effective way to improve gas-sensing properties. Noble metals [11-13] or oxides such as SnO_2 [14], TiO_2 [15], CuO [16], CeO_2 [17], Fe_2O_3 [18] were often used as dopants.

$ZnSnO_3$ thin films are usually fabricated by a variety of thin film deposition techniques, such as photo-atomic layer deposition [19], RF magnetron sputtering [20], chemical vapor deposition [21] and spray pyrolysis [22].The spray pyrolysis technique has several advantages over the above techniques such as simplicity, safety and low cost of the apparatus and the low cost of the raw materials. In this work, we shall deal with the electrical and gas sensing properties of $ZnSnO_3$ thin films prepared by spray pyrolysis process. The aim of this work is to determine the deposition condition of highly conductive transparent $ZnSnO_3$ thin films. In addition, influences of the iron doping treatment in a reducing atmosphere on properties of $ZnSnO_3$ thin films are investigated.

2. Preparation of iron doped perovskite $ZnSnO_3$ thin films

All the chemical reagents were analytically pure and used without further purification. Zinc chloride $ZnCl_4 \cdot 5H_2O$ (0.1 M) and stannic chloride $SnCl_4.5H_2O$ (0.1 M) with volume ratio 30:70 vol.% were dissolved in 100 ml of deionized water to give solution X. Different solution mixtures were prepared by drop wise adding 1 ml, 2.5 ml and 5 ml $FeCl_3 \cdot 4H_2O$ (0.1 M) solutions into the solution X. Each solution was stirred for one hour and was delivered to nozzle with constant and uniform flow rate of 5 ml/minute using air as a carrier gas. The spray (mist) produced by nozzle was sprayed onto the glass substrates heated at 400 ± 5^0C. Various parameters such as nozzle-to-substrate distance, deposition time, flow rate of solution, deposition temperature and concentration of source solution were optimized to obtain highly textured thin films of good quality. The 1 ml, 2.5 ml and 5 ml $FeCl_3$ added samples were referred as SF1, SF2 and SF3 respectively.

3. Material Characterization

As prepared films were characterized by X-ray diffractometer (RIGAKU-DMAX-2500) using CuKα (λ = 1.5418 Å) radiation with Ni filter in scanning angle of range 20-80 degree. The micro structural study was carried out using Transmission electron microscope (TEM). The TEM micrographs were obtained on a CM 200 Philips (200 kV HT) assembly. The quantitative elemental analysis of the films was estimated by computer controlled energy dispersive X- ray analyzer (model JEOL JSM-6360 Å) attached to the scanning electron microscope. The thickness and roughness of the films was carried out using surface profiler (Vetro Dectak-150). Electrical and gas sensing properties were measured using a static gas sensing system. The sensor performance on exposure of LPG, CO_2, hydrogen, ammonia, ethanol and chlorine was tested.

3.1 Crystal structure using X-ray diffraction

Figures 1 shows X-ray diffractogram of iron doped perovskite $ZnSnO_3$ thin films. The observed peaks are matching well with ASTM reported data [JCPD# 28-1486] of perovskite $ZnSnO_3$ thin films. There are no prominent peaks of Fe_2O_3 associated in XRD pattern. It may be due to smaller wt % of Fe_2O_3 as compared to $ZnSnO_3$. Increased grain size would be the reason of increase in the intensity. It reveals from XRD that the films are nanocrystalline in nature. The average grain sizes as determined from Scherer formula for each sample are presented in Table 1.

Sample name	Grain size calculated from XRD (nm)
SF1	24
SF2	21
SF3	26

Table 1: Grain size calculated from XRD

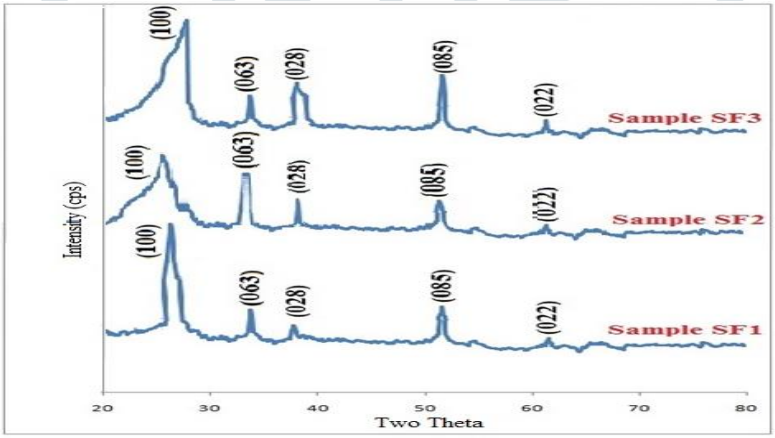

Fig. 1: X-ray diffraction spectra of sample SF1, SF2 and SF3.

Table 1 show the grain size of all samples calculated from XRD. The grain size of SF2 sample was lowest as compare to the grain size of SF1 and SF3 sample.

3.2 *Quantitative elemental analysis*

It is clear from the Table 2 that the SF1, SF2 and SF3 remain stoichiometric pervoskite. The increase in volume % of iron precursor ($FeCl_3 \cdot 4H_2O$) increases the mass % of Fe.

Sample Name	Quantity of solution (ml)	Mass % Zn	Sn	Fe	O	Total
SF1	101	18.69	19.86	0.78	61.67	101
SF2	102.5	18.59	19.72	2.37	61.82	102.5
SF3	105	18.67	19.46	4.82	62.05	105

Table 2: The composition of thin films SF1, SF2 and SF3.

3.3 Microstructural analysis

Figure 2 (a), 2 (b) and 2 (c) show the TEM images of powders [CM 200 Philips (200 kV HT)] of thin film samples SF1, SF2 and SF3 respectively. Each powder was dispersed in ethanol. Copper grid was used to hold the powder. All images show the particles to be spherical and nanocrystalline in nature. The particle size was observed to be increasing with the increase of volume % iron precursor in the base solutions of zinc and tin precursors. Table 3 show the average grain size of sample SF1, SF2 and SF3.

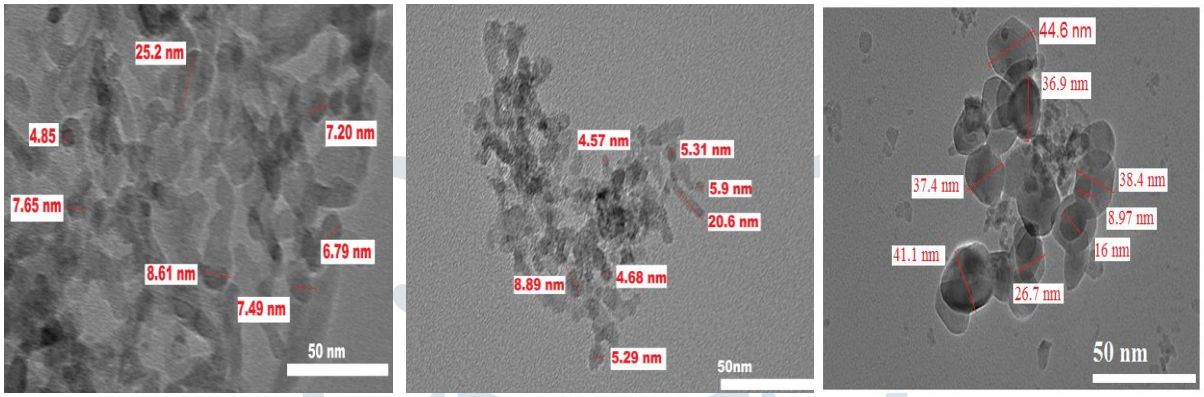

Fig. 2(a) **Fig**. 2(b) Fig.2(c)

Figure 2: TEM images (a) SF1, (b) SF2 and (c) SF3.

Sample name	Grain size (nm)
SF1	9.68 nm
SF2	8 nm
SF3	30 nm

Table3: Grain size

4 Electrical properties

4.1 *Electrical conductivity*

Temperature dependence electrical conductivity of thin film samples SF1, SF2 and SF3 are shown in figure 3. From figure 3, it is observed that conductivity increases with increase in temperature range from 100-450^{0}C for all samples. This increase in conductivity with increase of temperature is attributed to improvement of charge density and semiconducting behavior of the films. The modification causes the formation of heterogeneous intergrain boundaries of $ZnSnO_3$-Fe_2O_3. Due to temperature effect, the inter-grain boundary area decreases i.e. there is a decrease

in the scattering of the electron. Consequently, the carrier concentration and mobility in the inter-grain domains also increase. This in turn increases the conductivity.

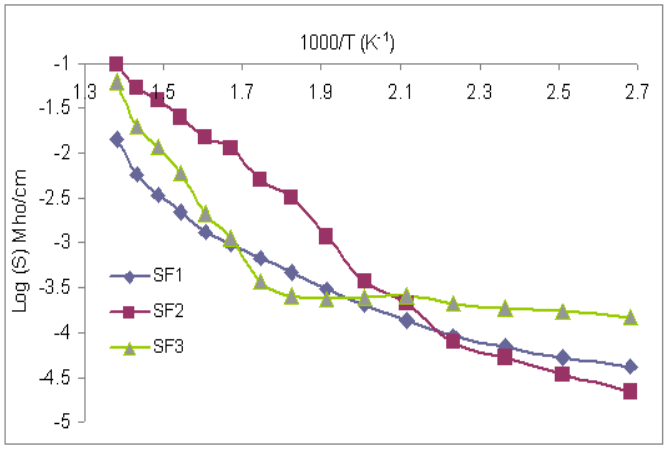

Fig.3

Fig. 3: Variation of electrical conductivity with temperature for SF1, SF2 and SF3 samples.

5. Gas sensing performance

5.1 *Gas response*

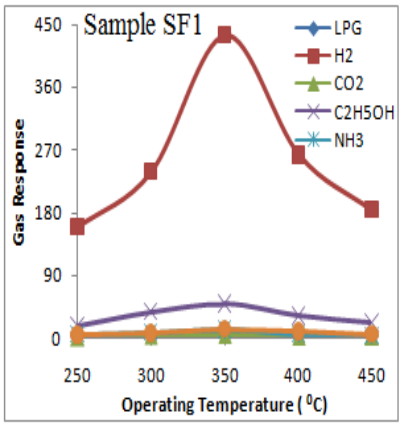

Fig.4 (a)

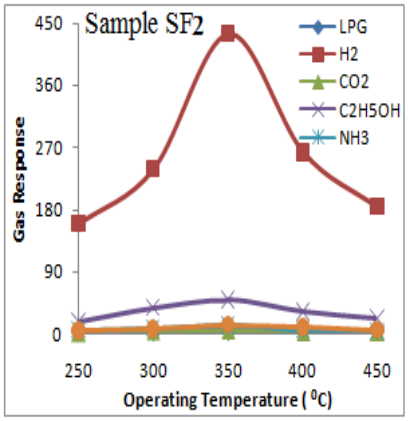

Fig.4 (b)

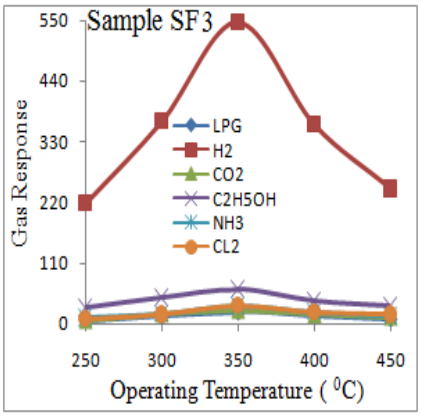

Fig.4 (c)

Fig.4: Gas response of: (a) SF1, (c) SF2 and (e) SF3.

The hydrogen gas response of iron doped perovskite $ZnSnO_3$ thin films are shown in figures 4 (a), (b) and (c). It is clear from figure that the nature of gas responses is similar for all gases. The response of hydrogen gas goes on increasing with increasing the operating temperature reaches to maximum at 350^0C and then decreases with further increase in the operating temperature.

5.2 Response and recovery

Figure 5 shows the variations in response to hydrogen (1000 ppm) with time for the iron doped perovskite $ZnSnO_3$ sample SF2 at 350 ^{0}C. The 90% response and recovery levels were attained within 14 and 18 second respectively. The very short response and recovery times are the important features of the sensor. This may be possible due to nanocrystalline nature of the films and high oxygen adsorption capability due to iron activator molecule on the surface and therefore fast reduction of exposed gas.

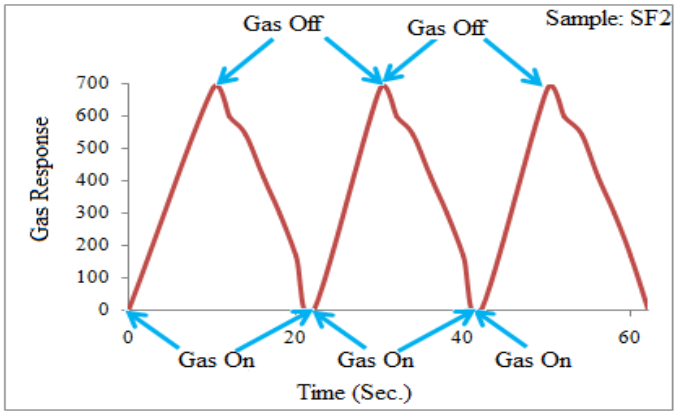

Fig.7: Response and recovery time

.

6. Discussion

In case of sensor SF1, SF2 and SF3, the adsorption-desorption sensing mechanism can be explained on the basis of reversible chemisorptions of the hydrogen on the iron doped $ZnSnO_3$ surface. It produces a reversible resistivity change with exchange of charges between hydrogen and iron doped $ZnSnO_3$ surface leading to change in the depletion width [23]. Gas sensing is based on interaction between the negatively charged oxygen adsorbed on the iron doped $ZnSnO_3$ surface and hydrogen to be detected. Initially molecular oxygen are adsorbed on the surface of iron doped $ZnSnO_3$ nanoparticles and electrons are consumed following the reactions:

$$O_{2\,(gas)} \leftrightarrow O_{2(ads)} \leftrightarrow O_{2(ads)} + e^- \leftrightarrow O_2^-{}_{(ads)}$$

Thus increase of the nanostructured film resistance. When the SF1, SF2 and SF3 sensor is exposed to reducing test gas hydrogen, its atom reacts with these chemisorbed oxygen ions and produce H_2O molecules consuming chemisorbed oxygen from film surface by releasing electrons. The sensing mechanism for hydrogen may be represented by following reaction:

$$(O^-)\, ZnSnO_3 + 2H \rightarrow H_2O(g) + e^-$$

$$2H_2 + O_2^-{}_{(ads)} \rightarrow 2H_2O + e^-$$

Considering $O^{2-}{}_{(ads)}$ as the predominant adsorbed species on SF1, SF2 and SF3 film surface, the electrons will be released back to the conduction band and will contribute to increase in the current through a nanorod. This also results in a reduction of surface depletion width and increase

conductivity. The reaction is exothermic in nature [24] and the molecular water desorbs quickly from the surface.

References

[1] C.Y.Lee, Y.S. Li, P.Lin and T.Y.Tseng, Journal of Nanoscience and Nanotechnology, **5** (2005)1088-1094.

[2] Y.J. Chen, Q.H. Li, S.Y. Lang,T.H. Wang, Q. Zhao and D.P. Yu, Applied Physics Letters, **85**(2004) 682-5684.

[3] S. Hoffmann, C. Ducati, B. Kleinsorge and J. Robertson, Applied Physics Letters, **83** (2003) 135-137.

[4] O.J. Lee, and K.H. Lee, Applied Physics Letters, **82** (2003)3770-3772.

[5] N.C. Xu, J. Tamaki, N. Miura and N. Yamazoe, Sensors and Actuators B **3** (1991)147-155.

[6] G. Zhang and M. Liu, Sensors and Actuators B **69** (2000)144-152.

[7] S. C. Navale, V. Ravi, I.S Mulla, S.W. Gosavi, S.K Kulkarni, Sensors and Actuators B **12** (2007) 38

[8] B.L. Zhu, C.S. Xie, A.H. Wang, J. Wu, R. Liu Wu, J. Liu, J. Mater. Science **42** (2007) 5416.

[9] T. Nenov, S. Yordanov, Sensors and Actuators B **8** (1992) 117.

[10] W.D. Zhang, W.H. Zhang, X.Y. Ma, J. Mater. Sci., **44** (2009) 3716.

[11] L.C. Tien, P.W. Sadik, D.P Norton, L.F Voss, S.J. Pearton, Appl. Phys. Lett., **87**(2005) 2106

[12] V.R. Shinde, T.P. Gujar, C.D. Lokhande, Sensors and Actuators B **123**(2007) 701.

[13] S.J. Chang, T.J. Hsueh, I.C Chen., S.F. Hsieh, S.P.Chang, C.L. Hsu, Y.R. Lin, B.R. Huang IEEE T Nano Tech. **7**(2008)754.

[14] K.W. Kim, P.S. Cho, S.J. Kim, J.H. Lee, C.Y. Kang, J.S. Kim, S.J. Yoon, Sensors and Actuators B **123**(2007) 318.

[15] B.L. Zhu, C.S. Xie, W.Y. Wang, K.J. Huang, J.H. Hu, Mater. Lett. **58**(2004) 624

[16] S. Aygu¨n, D. Cann, Sensors and Actuators B **106** (2005) 837.

[17] C.Q. Ge, C.S. Xie, S.Z. Cai, Mater. Sci. Eng.B **137**(2007) 53.

[18] H.X. Tang, M. Yan, H. Zhang, S.Z. Li, Ma X.F., Wang M., D.R. Yang, Sensors and Actuators B**114** (2006) 910.

[19] R.S. Niranjan, Y.K. Hwang, D.K. Kim, S.H. Jhung, J.S. Chang, I.S. Mulla, Mater. Chem. Phys. **92** (2005) 384-388.

[20] H.R. Kim, K.I. Choi, J.H. Lee, S.A. Akbar, Sensors and Actuators B **136** (2009) 138-143.

[21] K. Hieda, T. Hyodo, Shimizu Y., Egashira M., Sensors and Actuators B **133** (2008) 144-150.

[22] K.S. Yoo, S.H. Park, J.H. Kang, Sensors and Actuators B **108** (2005) 159-164.

[23] J. Xu, X. Jia, X. Lou and J. Shen, Solid State Electron. **50** (2006) 504

H. L. Hartnagel, A. L. Dawar, A. K. Jain, C. Jagadish, Semiconducting Transparent Thin Films, IOP, Bristol (1995) 231.

[24] O. Lupan, L. Chow, G.Y. Chai, B. Roldan, A. Naitabdi, Schulte A., Heinrich H., Mater. Science Eng. B, **145** (2007) 57- 66.